CURRENT SCIENCE AND TECHNOLOGY (CST)
VOL. 2, ISSUE 2, 29 – 34
DOI: https://doi.org/10.15282/cst.v2i2.9292

ORIGINAL ARTICLE

Phenothiazine-functionalized rGO for Electrochemical Capacitor

S.P. Lee[1,2], N.H.M. Saufi[1], E.Y.L. Teo[3], and K.F. Chong[1,2*]

[1]Faculty of Industrial Sciences and Technology, Universiti Malaysia Pahang, 26300 Pahang, Malaysia.
[2]Center for Advanced Intelligent Materials, Universiti Malaysia Pahang, 26600 Pahang, Malaysia.
[3]Department of Science and Technology, Universiti Putra Malaysia, 97008 Sarawak, Malaysia.

ABSTRACT – The functionalization arose as a technique to improve the physicochemical properties of the reduced graphene oxide (rGO) and consequently enhance the supercapacitor performance. The functionalization compound, phenothiazine (PTZ) introduces nitrogen and sulfur heteroatoms into rGO *via* the one-pot hydrothermal method at different mass ratio produced PTZ-rGO 5 and PTZ-rGO 10. Incorporation of PTZ on the rGO sheets in PTZ-rGO 5 contributes to the high surface area (163.49 m^2 g^{-1}) and pore volume (0.3187 cm^3 g^{-1}) properties. Contradictory, overloaded PTZ not only shows a lower reduction effect but also reduces the amount of PTZ functionalized in the PTZ-rGO 10 and consequently shows lower electrochemical performance. The excellent properties enable PTZ-rGO 5 enable it to achieve 119.5 F g^{-1} at 0.5 A g^{-1} for its specific capacitance and drive it to be the promising electrode material for supercapacitors.

ARTICLE HISTORY
Received: 14th Jan 2023
Revised: 15th May 2023
Accepted: 11th June 2023

KEYWORDS
Freeze-drying
Surface modification
EDLC
Pseudocapacitive
Redox activity

INTRODUCTION

Supercapacitors have become an emerging device in energy storage applications. The supercapacitor can be classified into two main categories, where the electrical double layer capacitive (EDLC) stores charge with the ions accumulation on the electrode material surface [1], while the pseudocapacitive store charge *via* redox reaction [2]. The synthesis of electrode material with the charge storage mechanism, which consists of the combination of EDLC and pseudocapacitive properties, has attracted attention in producing a high capacitance [3, 4] and durable supercapacitor [5, 6]. Therefore, nitrogen or sulfur-doped graphene becomes a suitable candidate for the electrode material. However, the synthesis method often requires high temperatures and complex experimental steps that are not feasible for all manufacturers [7, 8]. Polyaniline (PANI), as the nitrogen-containing molecule, is widely found as the rGO surface modification precursor to enhance electrochemical performance [6, 9, 10]. However, the PANI/rGO composite often required the PANI growth on GO using aniline monomer and subjected to hydrazine hydrate reduction to obtain PANI/rGO [11] or growth of PANI on readily reduced GO [12]. In the extend of our knowledge, there is still lack of the research for nitrogen and sulfur co-functionalization on rGO surface using a simple and one-pot method. Hence in this study, the nitrogen and sulfur-containing compound phenothiazine (PTZ) becomes the focused material to functionalize reduced graphene oxide (rGO) at different mass ratio and assess the electrochemical performance as electrode material. The findings belief to show and inspire other study to use the one-pot simple method as a favaourable approch in producing functionalized rGO.

MATERIALS AND METHODS

Preparation of PTZ-rGO Aerogel

A total of 40 mL of GO dispersion (4 mg mL^{-1}) prepared *via* modified Hummer's method as shown in the previous study [13]. The GO dispersion was added into 20 mL of PTZ solution (40 mg mL^{-1} in DMF) and mixed well before transfer into a Teflon-lined autoclave. The setup was heated at 180 °C for 6 hr, and the resultant product was washed with excess ethanol to remove unattached PTZ. Finally, the product was freeze-dried to obtain PTZ-rGO. The samples synthesized were designated as PTZ-rGO 5 and PTZ-rGO 10 for the mass ratio of PTZ to GO in 1:5 and 1:10, respectively. Figure 1 shows graphical summary of the preparation flow of PTZ-rGO aerogel.

*CORRESPONDING AUTHOR | K.F. Chong | ckfeng@ump.edu.my

Figure 1. Flow of preparation for PTZ-rGO aerogel synthesis.

Materials Characterization

The phase of the PTZ-rGO was identified using X-ray diffraction (XRD, Rigaku Miniflex II) at 2θ from 3° to 80°. The functionalities of PTZ-rGO were determined using Fourier transformed infrared spectroscopy (FTIR, PerkinElmer Spectrum 100) at wavenumber from 400 to 4000 cm^{-1}. The morphology and element composition of PTZ-rGO were investigated by scanning electron microscope with energy-dispersive X-ray analysis (SEM-EDX, FEI Quanta 450). The surface area and pores distribution of PTZ-rGO were analyzed with an N_2 adsorption-desorption isotherm (Micromeritics ASAP 2020) under 77 K at the degassing temperature of 120°C.

Electrochemical Measurement

The as-prepared PTZ-rGO was pressed on nickel foam to make a working electrode. Then, the electrochemical analysis was carried out in a three-electrode system (Autolab M101) with Ag/AgCl as the reference electrode and platinum wire as the counter electrode as shown in Figure 2. 5M KOH was used as the electrolyte for the entire electrochemical analysis consisting of cyclic voltammetry (CV), galvanostatic charge-discharge (GCD), and electrochemical impedance spectroscopy (EIS) analysis. The specific capacitance, C_{sp} was calculated as follows:

$$C_{sp} = \frac{I \times \Delta t}{m \times \Delta V} \quad (1)$$

where I is the discharge current applied, Δt is the duration needed to discharge completely, m is the mass of the sample, and ΔV is the potential window applied.

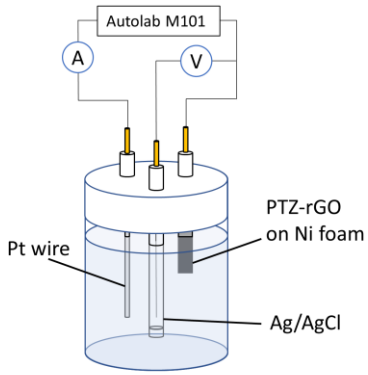

Figure 2. Three-electrode system setup for electrochemical measurement.

RESULTS AND DISCUSSION

Physicochemical Analysis

The PTZ-rGO was synthesized using the hydrothermal method at different mass loading of PTZ precursor. Figure 3(a) shows the XRD pattern of the PTZ-rGO and GO samples. Both the PTZ-rGO exhibit a significant peak at ca. 2θ = 25.8°, while GO shows a sharp peak at ca. 2θ = 10.1°. The significant peak shifted towards higher 2θ can be explained by the removal of oxygenated functionalities of GO during reduction *via* PTZ and causing a reduction of interlayer spacing from 8.8 to 3.5 Å. Although the PTZ-rGO only shows slightly greater interlayer spacing than graphite (2θ = 25.8°, 3.4 Å)[14], the incorporation of PTZ prevents the restacking of graphene sheets. As a result, it shows a quasi-broad peak (randomly arranged structure) compared to the orderly aligned graphite (highly crystalline structure). The removal of oxygenated functionalities is observed in the FTIR spectra, as shown in Figure 3(b). Generally, the GO and PTZ-rGO show a significant peak at ca. 1634 cm^{-1}, corresponding to the C=C bond of the GO/rGO plane. The diminished shoulder

peak at ca. 1744 cm^{-1} (C=O) indicates the reduction in PTZ-rGO samples. Interestingly, the FTIR peak at ca. 3456 cm^{-1} shows an increase in intensity in both PTZ-rGO samples due to the overlapping of the pyrrole-like N-H stretching of PTZ and remaining -OH stretching from the GO [15].

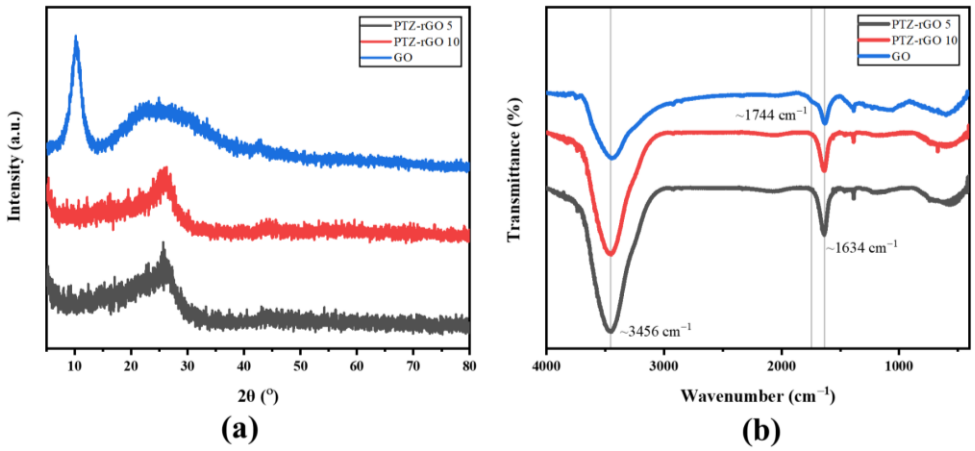

Figure 3. (a) XRD pattern of PTZ-rGO and GO; (b) FTIR spectra of PTZ-rGO and GO.

Figure 4 shows the morphology of PTZ-rGO samples under SEM analysis. Both samples exhibit interconnected pores, showing that the incorporation of PTZ plays a vital role in maintaining the porous structure of the PTZ-rGO. The smoother surface of the PTZ-rGO 10 compared to PTZ-rGO 5 can be explained by the less PTZ functionalized on the rGO surface, as observed in the EDX analysis. The elements detected and their weight percentage were summarized in Table 1. The distinct nitrogen and sulfur elements from PTZ are found to be 13.75 wt% and 12.87 wt%, respectively, in PTZ-rGO 5. This result shows PTZ-rGO 5 having more significant amounts of PTZ functionalized on rGO compared to PTZ-rGO 10 which only have 12.92 wt% of nitrogen and 11.01 wt% of sulfur. Such difference can be explained by the overloaded PTZ adverse functionalization effects where PTZ-to-rGO interaction is unable to withstand a load of multiple PTZ molecules (intermolecular interacted) at the localized point and washed off during the synthesis process. The oxygen content found to be lesser in PTZ-rGO 5 shows the greater reduction effect at the 1:5 mass ratio compared to PTZ-rGO 10, which is will be favorable for electrochemical study due to lower resistance for electron transfer.

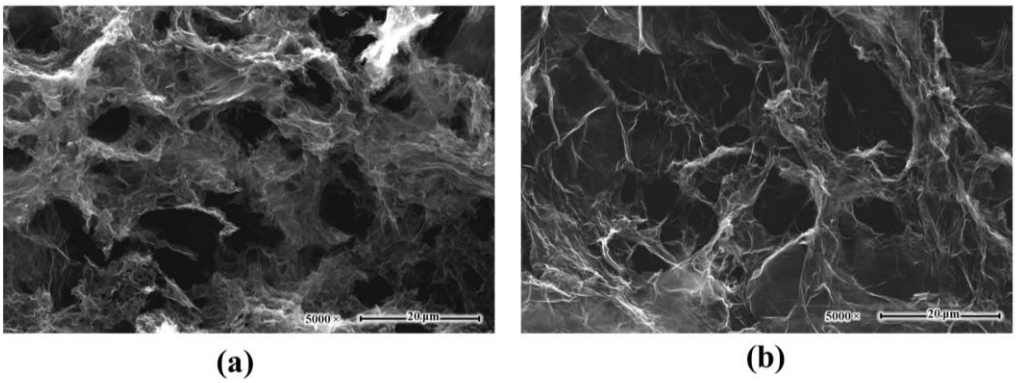

Figure 4. SEM images of (a) PTZ-rGO 5 and (b) PTZ-rGO 10 at the magnification of 5000×.

Table 1. Elemental analysis of the PTZ-rGO samples.

Element	PTZ-rGO 5 (wt%)	PTZ-rGO 10 (wt%)
C	68.47	70.27
N	13.75	12.92
O	4.91	5.80
S	12.87	11.01

Figure 5(a) shows the N_2 adsorption-desorption isotherm for PTZ-rGO and GO. The PTZ-rGO samples are classified as Type II isotherms, which can further be interpreted as macroporous or non-porous materials [16]. The monolayer adsorption of the N_2 gaseous molecule occured at the low p/p° region (<0.2) and was followed by multilayer adsorption at the high p/p° region. PTZ-rGO 10 shows a more mesoporous and macroporous structure compared to PTZ-rGO 5 due to the washed-off of the PTZ as hypothesized with the EDX analysis leaving the larger pore size of the PTZ-rGO structure. This pore distribution as shown in Figure 5(b) contributes by each of the PTZ-rGO reflect their surface area at 163.49 $m^2\ g^{-1}$ and 731.36 $m^2\ g^{-1}$, while pore volume at 0.3187 $cm^3\ g^{-1}$ and 1.1854 $cm^3\ g^{-1}$ representing PTZ-rGO 5 and

PTZ-rGO 10, respectively. This increment in surface area compared to GO (14.94 m^2 g^{-1} and 0.0359 cm^3 g^{-1}) further shows the role of PTZ in enhancing the surface area *via* functionalized on the rGO surface.

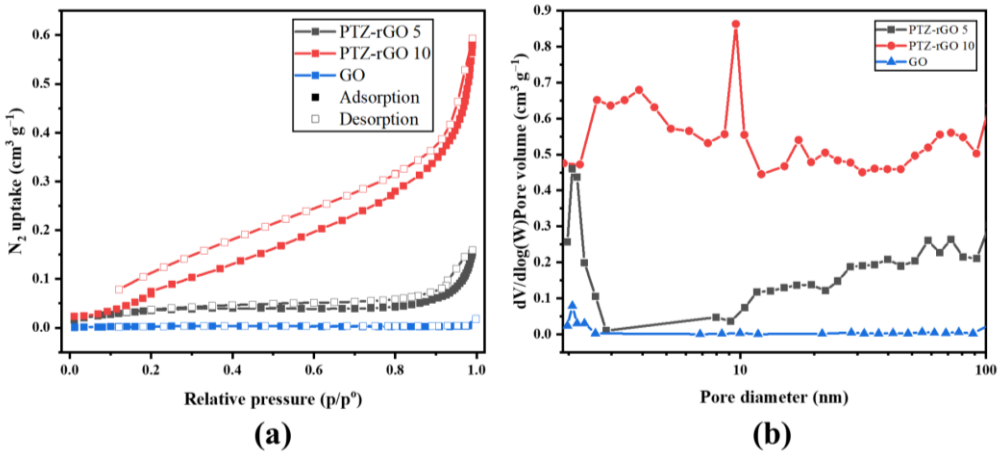

Figure 5. (a) N_2 adsorption-desorption isotherm and (b) pore size distribution of PTZ-rGO and GO.

Electrochemical Performance

PTZ-rGO samples were examined for their electrochemical performance with cyclic voltammetry (CV), galvanostatic charge-discharge (GCD), and electrochemical impedance spectroscopy (EIS) in a three-electrode system where platinum wire and Ag/AgCl as counter and reference electrode. CV curve as shown in Figure 6(a) having both PTZ-rGO 5 and PTZ-rGO 10 show a quasi-rectangular shape (EDLC properties) with broad doublet redox peaks at ca. −0.35 V and −0.6 V. These broad peaks contributed by the pseudocapacitive effect from the incorporation of PTZ at the rGO surface [17]. The EDLC effect becomes dominant at a high scan rate due to the limited duration for electron transfer between the PTZ and the electrolyte.

The GCD analysis in Figure 6(b) shows a linear charge and discharge line with a slight curvature at the redox peak potential as observed in CV. The curvature of the GCD curve becomes significant when a tremendous PTZ amount has functionalized on rGO (more significant pseudocapacitive effect), which well corroborates with the CV curve and EDX findings. The synergistic effect of EDLC and pseudocapacitive properties of PTZ-rGO 5 enable it to show good specific capacitance, C_{sp} of 119.5 F g^{-1} at 0.5 A g^{-1} compared to PTZ-rGO 10 (91.0 F g^{-1}). Figure 6(c) shows the C_{sp} at different current densities applied for PTZ-rGO 5 and 10, where the significant increase of the C_{sp} value at the low current density region and less C_{sp} increment in the high current density region further reflect the pseudocapacitive effect of the PTZ-rGO samples.

Figure 6(d) shows the Nyquist plot of the PTZ-rGO with the inset as the magnification at the low Z' region and the Randles equivalent circuit used for the curve fitting. The equivalent circuit fitted consists of an R_s (electrolyte, internal electrode, and contact resistance) connected in series to charge transfer resistance, R_{ct}, and constant phase element, CPE1 (EDLC), while CPE2 (pseudocapacitive) is connected in series with R_{ct} [18]. The Warburg impedance, W, was connected in the parallel joint with CPE1 and CPE2. Table 2 summarized the results of each parameter fitted with the equivalent circuit. The lower R_s and R_{ct} value of the PTZ-rGO 5 (598.4mΩ and 1.186 mΩ), further supports the excellent electrochemical performance compared to PTZ-rGO 10 (652.3 mΩ and 74.29 Ω), which reflects the vital role of the PTZ in contributing to the charge storage performance. The greater W value in PTZ-rGO 5 also shows the better diffusion of the electrolyte for charge storing compared to PTZ-rGO 10 which again contributed by the greater amount of PTZ functionalized on the rGO surface.

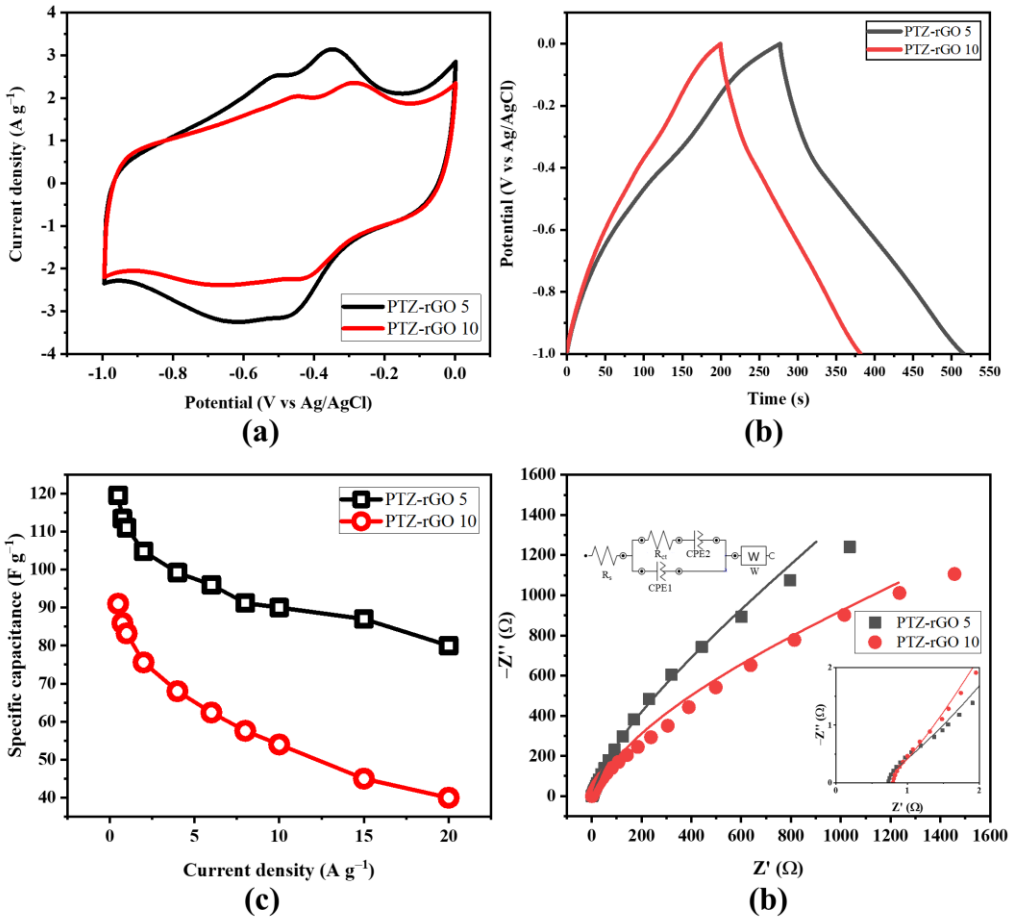

Figure 6. (a) CV curve, (b) GCD curve, (c) C_{sp} value at different current densities, and (d) Nyquist plot for PTZ-rGO (inset as low Z' region and equivalent circuit fitted).

Table 2. Fitted equivalent circuit paramters with data of the PTZ-rGO samples.

Parameters	PTZ-rGO 5	PTZ-rGO 10
R_s (Ω)	0.5984	0.6523
R_{ct} (Ω)	0.001186	74.294
CPE1 (Mho·s^N)	0.002582	0.001819
N_{CPE1}	0.5106	0.9146
CPE2 (Mho·s^N)	0.003367	0.001483
N_{CPE2}	1.0969	0.3348
W (Mho·$s^{1/2}$)	0.01968	0.01838
χ^2	0.1416	0.2022

CONCLUSION

The incorporation effect of PTZ onto rGO sheets was studied for its application as a supercapacitor electrode material. The excessive loading of PTZ adversely affects GO reduction and the electrochemical performance as electrode material. The synergistic effect of EDLC (by rGO) and pseudocapacitive (by PTZ) of PTZ-rGO 5 with its higher amount of PTZ incorporated has contributed to the highest specific capacitance of 119.5 F g^{-1} at 0.5 A g^{-1} due to its excellent charge transfer resistance (1.186 mΩ). This study highlights the simple one-pot hydrothermal method in rGO surface modification *via* nitrogen and sulfur functionalization for supercapacitor applications.

ACKNOWLEDGEMENT

The authors would like to acknowledge the funding from the Ministry of Education Malaysia in the form of FRGS [RDU1901186:FRGS/1/2019/STG07/UMP/02/6].

REFERENCES

[1] S.B. Aziz, A.S.F.M. Asnawi, R.T. Abdulwahid, H.O. Ghareeb, S.M. Alshehri, T. Ahamad, J.M. Hadi, M.F.Z. Kadir, Design of potassium ion conducting PVA based polymer electrolyte with improved ion transport properties for EDLC device application, Journal of Materials Research and Technology, 13 (2021) 933-946.
[2] A. Djire, P. Pande, A. Deb, J.B. Siegel, O.T. Ajenifujah, L. He, A.E. Sleightholme, P.G. Rasmussen, L.T. Thompson, Unveiling the pseudocapacitive charge storage mechanisms of nanostructured vanadium nitrides using in-situ analyses, Nano Energy, 60 (2019) 72-81.
[3] J. Wang, S. Dong, B. Ding, Y. Wang, X. Hao, H. Dou, Y. Xia, X. Zhang, Pseudocapacitive materials for electrochemical capacitors: from rational synthesis to capacitance optimization, Natl. Sci. Rev., 4 (2017) 71-90.
[4] Z. Bo, X. Lu, H. Yang, S. Wu, X. Cheng, B. Gong, Z. Huang, J. Yan, K. Cen, K. Ostrikov, Surface-dominant pseudocapacitive supercapacitors with high specific energy and power for energy storage, Journal of Energy Storage, 42 (2021) 103084.
[5] M.H. Hamsan, S.B. Aziz, M.F.Z. Kadir, M.A. Brza, W.O. Karim, The study of EDLC device fabricated from plasticized magnesium ion conducting chitosan based polymer electrolyte, Polymer Testing, 90 (2020) 106714.
[6] S.B. Aziz, E.M.A. Dannoun, M.H. Hamsan, R.T. Abdulwahid, K. Mishra, M.M. Nofal, M.F.Z. Kadir, Improving EDLC Device Performance Constructed from Plasticized Magnesium Ion Conducting Chitosan Based Polymer Electrolytes via Metal Complex Dispersion, Membranes, 11 (2021).
[7] M.B. Arvas, M. Gencten, Y. Sahin, One-step synthesized N-doped graphene-based electrode materials for supercapacitor applications, Ionics, 27 (2021) 2241-2256.
[8] M.B. Arvas, H. Gürsu, M. Gencten, Y. Sahin, Preparation of different heteroatom doped graphene oxide based electrodes by electrochemical method and their supercapacitor applications, Journal of Energy Storage, 35 (2021) 102328.
[9] K.T. Kubra, R. Hafeez, G. Ali, H. Ahmad, A. Butt, A. Salman, R. Sharif, M. Sultana, M. Bashir, Electrochemical investigation of a novel quaternary composite based on dichalcogenides, reduced graphene oxide, and polyaniline as a high-performance electrode for hybrid supercapacitor applications, Journal of Alloys and Compounds, 909 (2022) 164854.
[10] E. Salehi, H. Ghafouri Taleghani, M. Soleimani Lashkenari, M. Ghorbani, Synthesis and electrochemical properties of polyaniline/S-Rgo nanocomposites with different S-rGO contents for hybrid energy storage devices, Journal of Electroanalytical Chemistry, 909 (2022) 116138.
[11] M. Ates, M. Yildirim, The synthesis of rGO/RuO2, rGO/PANI, RuO2/PANI and rGO/RuO2/PANI nanocomposites and their supercapacitors, Polymer Bulletin, 77 (2020) 2285-2307.
[12] X. Zhang, B. Li, T. Chen, X. Ke, R. Xiao, Study on CePO4 modified PANI/RGO composites to enhance the anti-corrosion property of epoxy resin, Progress in Organic Coatings, 178 (2023) 107472.
[13] S.P. Lee, G.A.M. Ali, H. Algarni, K.F. Chong, Flake size-dependent adsorption of graphene oxide aerogel, Journal of Molecular Liquids, 277 (2019) 175-180.
[14] H. Zheng, Y. Cheng, R. Zhao, Y. Ye, J. Chen, An improved strategy to synthesize graphite oxide with controllable interlayer spacing as coatings for anticorrosion application, Journal of Applied Polymer Science, 138 (2021) 49823.
[15] M.U. Khan, R.A. Rather, Z.N. Siddiqui, Design, characterization and catalytic evaluation of halometallic ionic liquid incorporated Nd2O3 nanoparticles ([smim][FeCl4]−@Nd2O3) for the synthesis of N-aryl indeno pyrrole derivatives, RSC Advances, 10 (2020) 44892-44902.
[16] K.A. Fayemiwo, G.T. Vladisavljević, S.A. Nabavi, B. Benyahia, D.P. Hanak, K.N. Loponov, V. Manović, Nitrogen-rich hyper-crosslinked polymers for low-pressure CO2 capture, Chemical Engineering Journal, 334 (2018) 2004-2013.
[17] K. Surya, M.S. Michael, Pseudocapacitive binary metal oxide NiMn2O4 nanoparticles as an electrode for high-powered hybrid supercapacitors, Journal of Materials Science: Materials in Electronics, 33 (2022) 3139-3150.
[18] S.P. Lee, G.A.M. Ali, H.H. Hegazy, H.N. Lim, K.F. Chong, Optimizing Reduced Graphene Oxide Aerogel for a Supercapacitor, Energy & Fuels, 35 (2021) 4559-4569.